processes

MDPI

Article

Temperature Prediction Model for Horizontal Shale Gas Wells Considering Stress Sensitivity

Jianli Liu [1], Fangqing Wen [2], Hu Han [3], Daicheng Peng [4], Qiao Deng [3,*] and Dong Yang [3,*]

[1] School of Mechanical Engineering, Yangtze University, Jingzhou 434023, China; jianli.liu@yangtzeu.edu.cn
[2] Hubei Key Laboratory of Intelligent Vision Based Monitoring for Hydroelectric Engineering, China Three Gorges University, Yichang 443002, China; wfqltt@163.com
[3] School of Petroleum Engineering, Yangtze University, Wuhan 430102, China; hancupb@126.com
[4] Key Laboratory of Exploration Technologies for Oil and Gas Resources, Yangtze University, Ministry of Education, Wuhan 430100, China; pengdc_geo@126.com
* Correspondence: dongyang@yangtzeu.edu.cn (D.Y.); dengqiao@yangtzeu.edu.cn (Q.D.)

Abstract: In the production process of horizontal wells, wellbore temperature data play a critical role in predicting shale gas production. This study proposes a coupled thermo-hydro-mechanical (THM) mathematical model that accounts for the influence of the stress field when determining the distribution of wellbore temperature. The model integrates the effects of heat transfer in the temperature field, gas transport in the seepage field, and the mechanical deformation of shale induced by the stress field. The coupled model is solved using the finite difference method. The model was validated against field data from shale gas production, and sensitivity analyses were conducted on seven key parameters related to the stress field. The findings indicate that the stress field exerts an influence on both the wellbore temperature distribution and the total gas production. Neglecting the stress field effects may lead to an overestimation of shale gas production by up to 12.9%. Further analysis reveals that reservoir porosity and Langmuir volume are positively correlated with wellbore temperature, while permeability, Young's modulus, Langmuir pressure, the coefficient of thermal expansion, and adsorption strain are negatively correlated with wellbore temperature.

Keywords: distributed temperature sensing; stress sensitivity; thermo-hydro-mechanical; temperature modeling

check for updates

Academic Editor: Qingbang Meng

Received: 7 May 2025
Revised: 4 June 2025
Accepted: 13 June 2025
Published: 15 June 2025

Citation: Liu, J.; Wen, F.; Han, H.; Peng, D.; Deng, Q.; Yang, D. Temperature Prediction Model for Horizontal Shale Gas Wells Considering Stress Sensitivity. *Processes* **2025**, *13*, 1896. https://doi.org/10.3390/pr13061896

Copyright: © 2025 by the authors. Licensee MDPI, Basel, Switzerland. This article is an open access article distributed under the terms and conditions of the Creative Commons Attribution (CC BY) license (https://creativecommons.org/licenses/by/4.0/).

1. Introduction

As conventional fossil energy resources diminish and energy demand escalates, the efficient and sustainable advancement of unconventional fossil fuels such as shale gas, along with other geological energy resources, has emerged as a focal point for scientific inquiry and industrial development [1,2]. Geological energy encompasses various forms, including conventional sources like coal, oil, and natural gas, alongside unconventional sources such as shale gas and coal-bed methane [3,4]. Shale gas has garnered significant attention in recent years due to its substantial reserves and extensive geographical spread [5]. Shale gas mostly resides in dense shale formations, and its extraction not only offers a novel solution to the imbalance between energy supply and demand but also significantly contributes to the diversification of the global energy landscape.

Shale gas resources are more difficult to extract compared to traditional oil and gas reservoirs due to their ultra-low permeability and low porosity features [6–8]. Horizontal well multistage fracturing technology has become one of the primary ways to develop

unconventional oil and gas resources and boost recovery [9–11]. Accurately comprehending the quantity and spatial distribution of hydraulic fractures is vital for guiding and improving the development of oil and gas reservoirs. In this regard, modern technologies such as Distributed Temperature Sensors have been widely deployed in numerous fields. Shell pioneered the use of fiber-optic temperature sensors in the oil sector to achieve continuous downhole temperature monitoring with a certain degree of accuracy [12–14]. DTS technology not only provides real-time data for identifying, quantifying, and analyzing near-wellbore fracture geometries, fracking fluid distributions, and the overall production enhancement effect but also facilitates the monitoring and optimization of production dynamics [15]. Tabatabaei et al. used distributed temperature sensing technology to observe dynamic temperature profiles along a wellbore during real-time fracturing [16]; Kaeshkov et al. measured transient temperature profiles via fiber-optic distributed sensors [17]. Malanya et al. determined fracture locations before, during, and after hydraulic fracturing based on DTS data [18]; Wei et al. proposed a transient multiphase flow and heat transfer modeling framework, which improved the average relative error of annular fluid temperature estimation by 13% [19]. Yan et al. combined DTS monitoring technology with an innovative fracturing method to effectively optimize the fracturing strategy, which ultimately improved hydrocarbon recovery in tight reservoirs [20].

A quantitative analysis of fluid flow profiles utilizing temperature data received from distributed temperature sensors necessitates the building of related mathematical models [21]. Currently, a variety of temperature prediction models have been presented by researchers for multistage horizontal wells in hydraulic fracturing. Among these, Ramey first proposed a prediction model for predicting the evolution of the temperature field with time and depth in single-phase fluids in vertical wells, which laid a theoretical foundation for the wellbore temperature model [22]. Luo et al. further added the microthermal impacts of non-Darcy flow and fractures around a wellbore into the research scope and studied their impact on the temperature distribution of the wellbore [23]. Cui et al. suggested a temperature prediction model for the temperature of horizontal wells for dynamic monitoring and fracture diagnosis [24]. Yang et al. studied the dynamic change features of fracture temperature during fracturing, closure, and flowback [25]. In addition, Sui explored thermodynamic behavior during the completion of exposed hole packers in tight gas reservoirs by creating a semi-analytical reservoir–wellbore coupled thermal model [26]. On this premise, Cao devised a linked thermal-water mathematical model to predict the production process of single-phase multistage hydraulic fracturing horizontal wells in confined reservoirs [27]. However, at present, the forward temperature prediction models of multistage fractured horizontal wells are primarily based on the study framework of thermo-hydro coupling, and the stress sensitivity characteristics of reservoirs are less explored. Zheng et al. experimentally found that the permeability of a shale matrix showed significant stress sensitivity under both low and high perimeter pressure conditions [28]. Wu et al. showed that the smaller the modulus of elasticity of shale, the higher its compressibility, which led to an increase in stress sensitivity [29]. In addition, Li et al. also pointed out that the stress sensitivity of shale is closely related to its mechanical properties, including mineral composition and rock mechanical properties [30]. The multi-physical field coupling impact of the thermo-hydro-mechanical process has not been systematically introduced. This shortcoming limits the application of the model under complex reservoir conditions and needs further investigation and development.

This study establishes a thermo-hydro-mechanical coupled mathematical model to predict the temperature distribution in multistage fractured horizontal wells during production, taking into account heat conduction, heat convection, stress-sensitive effects, and minor fluctuations of the Joule–Thomson effect. Simultaneously, the impact of reservoir

stress-sensitive factors on wellbore temperature distribution is thoroughly examined, offering a theoretical foundation for the interpretation and utilization of temperature data in horizontal wells.

2. Physical Model

Natural gas in shale reservoirs consists primarily of free gas in the pores or natural fractures and adsorbed gas in the shale matrix. During the production process, gas travel involves several scales, and the transport at different scales may exhibit variable temperature change characteristics. Based on this, this paper presents a multiscale temperature conceptual model (shown in Figure 1). The model models the flow and heat transfer behaviors of the formation, fractures, and wellbore in a unified way through a multiscale coupling approach and combines these with distributed temperature sensing technology to provide a comprehensive research framework and theoretical basis for the flow mechanism, fracture distribution, and coupled thermo-hydro-mechanical behavior during shale gas extraction. Figure 1a displays a complete shale gas reservoir model, including the formation model, fracture model, and wellbore model. Figure 1b displays the distribution of multistage fracturing around the wellbore. To simplify the modelling, straight line fracturing was used to represent the fracture network formed after hydraulic fracturing. As illustrated in Figure 1c, the process of heat transfer between the wellbore and the fracture and formation is depicted. The transfer of heat comprises two distinct processes: conduction, which occurs between the formation and the wellbore, and convection, which occurs between the fracture and the wellbore. These processes collectively influence the distribution of wellbore temperature. As illustrated schematically in Figure 1d, shale gas migrates from a fracture to the wellbore. The figure employs the use of blue arrows, which point from the fracture region to the wellbore, thus indicating that fluids are converging towards the wellbore under the influence of driving differential pressure.

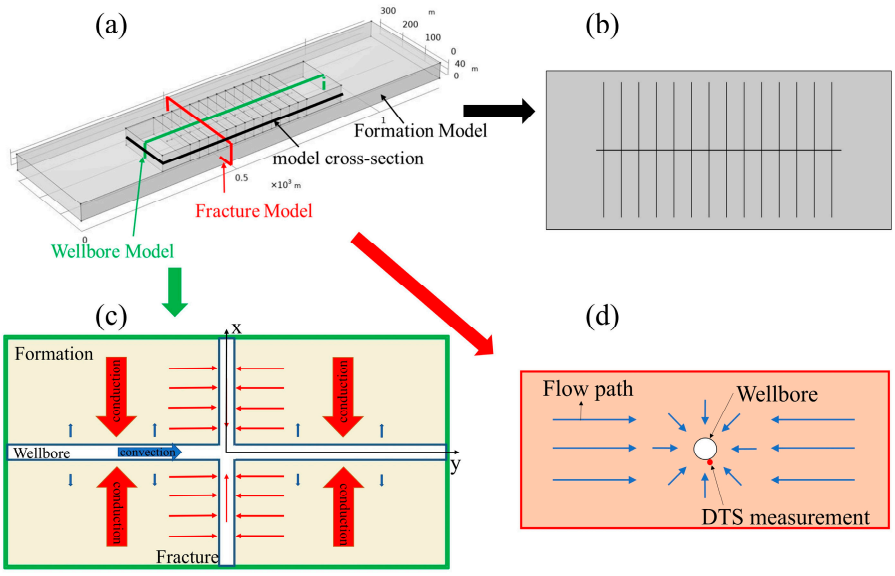


Figure 1. Schematic structure of wellbore temperature monitoring for multistage fractured horizontal wells for shale gas. (**a**) Reservoir, wellbore, and fracture coupling model. (**b**) Cross-section of reservoir, wellbore, and fracture. (**c**) Heat exchange in wellbore, and fracture; (**d**) Flow path near the wellbore along a hydraulic fracture.

3. Mathematical Modeling

To build a temperature forecast model for horizontal wells, a full-coupled mathematical model of shale deformation, gas flow, and heat transfer was defined and presented based

on porous elasticity theory, Darcy's law, and heat transfer methods [31]. The derivation of the model is based on the following assumptions: (1) shale is regarded as an isotropic homogeneous elastic medium consisting of a matrix, pores, and cracks; (2) the gas in the cracks exists in a free state and its flow behavior follows Darcy's law; (3) the gas in the matrix coexists in both free and adsorbed states, and the flow of the gas in a free state exhibits the Knudsen diffusion characteristics; (4) the desorption kinetics of the adsorbed state shale gas in the matrix can be described by Langmuir's isothermal adsorption law; (5) the gas reservoir is in equilibrium before exploitation and dynamic equilibrium is maintained between the adsorbed and free state gases; and (6) the gas flow is a single-phase isothermal seepage process, and the effect of gravity is neglected [32].

3.1. Deformation Control Equations

In a homogeneous and isotropic porous medium, the strain–displacement relationship of the shale matrix can be expressed by the following equation [33]:

$$\varepsilon_{ij} = \frac{1}{2}(u_{i,j} + u_{j,i}) \tag{1}$$

where ε_{ij} is the strain tensor component and u_i is the displacement component. Since the inertial forces are neglected, the stress balance equation for the shale matrix can be expressed as follows [34]:

$$\sigma_{ij,j} + f_i = 0 \tag{2}$$

where σ_{ij} is the stress tensor component and f_i is the volumetric force component.

According to the porous elasticity theory, the stress–strain relationship of isothermal linear elastic porous media can be deduced from the reservoir pressure (effective stress), temperature change, and strain caused by the desorption of shale gas in the process of shale gas extraction, and its expression is as follows [35]:

$$\varepsilon_{ij} = \frac{1}{2G}\sigma_{ij} - \left(\frac{1}{6G} - \frac{1}{9K}\right)\sigma_{kk}\delta_{ij} + \frac{\alpha}{3K}p\delta_{ij} + \frac{\alpha_T}{3}(T - T_0)\delta_{ij} + \frac{\varepsilon_s}{3}\delta_{ij} \tag{3}$$

where $G = E/2(1 + \nu)$ is the shear modulus of shale, in units of GPa; ν is the Poisson's ratio; E is the elastic modulus of shale, in units of GPa; $K = E/3(1 - 2\nu)$ is the bulk modulus of shale, in units of GPa; ε_s is the matrix contraction strain caused by shale gas desorption; α_T is the thermal expansion coefficient, in units of K^{-1}; T is the temperature variable, in units of K; T_0 is the initial temperature, in units of K; and p is the gas pressure within the matrix, in units of Pa. The trace of the stress tensor is denoted as $\sigma_{kk} = \sigma_{11} + \sigma_{22} + \sigma_{33}$ and δ_{ij} is the Kronecker delta, which equals 1 when $i = j$ and 0 otherwise. By combining Equations (1)–(3), the modified Navier equation can be derived based on the external reservoir pressure (effective stress), thermal expansion, and strain caused by shale gas desorption [35].

$$Gu_{i,jj} + \frac{G}{1 - 2v}u_{j,ji} - \alpha p_{,i} - K\alpha_T T_{,i} - K\varepsilon_{s,i} + f_i = 0 \tag{4}$$

Equation (4) is the governing equation of shale deformation. The parameter $\alpha p_{,i}$ signifies the impact of fluid seepage on the deformation of the rock mass, while $K\alpha_T T_{,i}$ denotes the effect of temperature change on the deformation of the rock mass. Furthermore, $K\varepsilon_{s,i}$ reflects the effect of shale gas desorption strain on the deformation of the rock mass.

3.2. Gas Flow Equation

Shale gas exists in different forms in matrices and fractures [36], and its transport mechanism varies depending on the form. In a matrix, shale gas exists mainly in an

adsorbed state, while in fractures it exists mainly in a free state [37]. Therefore, the effects of viscous flow, Knudsen diffusion, and adsorption/desorption processes must be considered together when establishing the continuity equation for shale gas. According to the mass balance principle, the continuity equation of shale gas can be expressed as follows [38]:

$$\frac{\partial}{\partial t}\left[\rho_g \phi + (1-\phi) m_{ads}\right] + \nabla \cdot q_m = 0 \tag{5}$$

where ρ_g is the gas density, ϕ is the porosity of the porous medium, and q_m is the Darcy velocity vector [39].

$$q_m = -\frac{\rho_m k_{m0}}{\mu_g}\nabla p_m - M_g D_{km}\nabla C_m = -\frac{\rho_m k_{m0}}{\mu_g}\nabla p_m - \frac{\rho_m D_{km}}{p_m}\nabla p_m = -\frac{\rho_m k_m}{\mu_g}\nabla p_m \tag{6}$$

where ρ_m is employed to denote matrix density, k_{m0} is used to denote matrix initial permeability, p_m is used to denote pore pressure, μ_g is used to denote matrix gas viscosity, C_m represents the molar concentration of the gas (mol/m^3), and D_{km} denotes the diffusion coefficient of the matrix [40]. The quantity k_{m1} is defined as the matrix permeability, which can be expressed as follows:

$$k_{m1} = k_{m0}\left(1 + \frac{\mu_g D_{km}}{p_m k_{m0}}\right) \tag{7}$$

In the gas transportation process, when the mean free path of gas molecules and the pore diameter of the porous medium reach a comparable order of magnitude, the Knudsen diffusion effect will appear. In terms of the microscopic pore structure of shale gas reservoirs, the pore diameters of shale gas reservoirs are mainly distributed in the range of 4 nm to 200 nm [40], which is similar to the mean free path of methane molecules in terms of scale characteristics. Given this, the Knudsen diffusion mechanism occupies an important position in the gas transport process of shale gas reservoirs, and its role should not be ignored. The gas flux due to Knudsen diffusion can be expressed according to the relevant theory [41]:

$$N_k = -M_g D_{km}\nabla C_m = -M_g D_{km}\nabla\left(\frac{p}{ZRT}\right) = -\frac{\rho_m D_{km}\nabla p}{p} \tag{8}$$

It is possible to represent D_{km} as follows:

$$D_{km} = \frac{4 k_{mi} c_k}{2.81708\sqrt{\frac{k_{mi}}{\phi_m}}}\sqrt{\frac{\pi RT}{2M_g}} \tag{9}$$

where ϕ_m is the matrix porosity; R is the generic gas coefficient; and c_k is the constant 1, which is dimensionless [39].

Taking into account the effects of viscous flow, Knudsen diffusion, adsorption/desorption processes, and thermal expansion effects, the effective permeability of the shale matrix can be expressed as follows:

$$k_m = k_{m1}\exp\left(\left(-1+\frac{1}{\phi_0}\right)\left(\frac{p-p_0}{K_s} - \alpha_T T(T-T_0) + \varepsilon_v - \left(\frac{V_L p}{p+P_L} - \frac{V_L p_0}{p_0+P_L}\right)\right)\right)^3 \tag{10}$$

In the gas absorption process, the mass of the absorbed gas molecules can be expressed as follows [42]:

$$m_{ads} = \rho_s \rho_{ga} V_E \tag{11}$$

The standard volume of gas adsorbed per unit rock mass can be expressed as follows:

$$V_E = \frac{pV_L}{p + P_L} \tag{12}$$

where V_L is the Langmuir volume, with units in m^3/Kg; P_L is the Langmuir pressure (the pressure at which the adsorbed gas content equals $V_L/2$), with units in Pa; ρ_s is the bulk density of the rock, with units in kg/m^3; ρ_{ga} is the gas density at standard conditions, with units in kg/m^3; and V_E is the adsorption isotherm function.

The field gas density can be calculated from the true gas equation of state:

$$\rho_g = \frac{pM_g}{ZRT} \tag{13}$$

where M_g is the molecular weight of the gas, R is the universal gas constant, and T is the absolute temperature. The compression factor Z is based on the proposed critical pressure (p_{pr}) and proposed critical temperature (T_{pr}) of the gas mixture, calculated by correlation [43].

$$Z = \left(0.702e^{-2.5T_{pr}}\right)\left(p_{pr}^2\right) - \left(5.524e^{-2.5T_{pr}}\right)\left(p_{pr}\right) + \left(0.044T_{pr}^2 - 0.164T_{pr} + 1.15\right) \tag{14}$$

Among the many gas properties, gas viscosity is usually characterized by certain correlation equations. The value of gas viscosity plays an important role in modeling the mobility of the gas in the reservoir and significantly affects the accurate estimation of the reserves. For this reason, the correlation equation proposed by Lee et al. was modified [44].

$$\begin{cases} \mu_g = 10^{-7}Ke^{X(0.001\rho_g)^Y} \\ K = \frac{(22.7+48.3M_g)T^{1.5}}{209+1900M_g+1.8T} \\ X = 3.5 + 547.8/T + 10M_g \\ Y = 2.44 - 0.22X \end{cases} \tag{15}$$

By substituting Equations (6), (10), (11), (13), and (15) into Equation (5), the following results can be obtained:

$$\left[\frac{M_g}{ZRT}\phi + (1-\phi)\frac{M_g\rho_s V_L P_L}{(p+P_L)^2} + \phi/K_s\right]\frac{\partial p}{\partial t} - \nabla\cdot\left(\frac{k_{app}}{\mu}\nabla p\right) = Q_s \tag{16}$$

3.3. Temperature Governing Equation

The temperature evolution during shale gas extraction can be characterized by the temperature field model, which depicts the dynamic changes of temperature over time and spatial distribution in detail. Based on the principle of energy conservation, a transient reservoir thermal model is constructed in this study, which comprehensively incorporates a variety of trace thermal effects on the temperature profile, including but not limited to heat conduction, heat convection, the Joule–Thomson effect, viscous dissipation, and thermal expansion effects. To deeply analyze the thermodynamic behavior during shale gas extraction, we further developed thermodynamic sub-models for the reservoir, hydraulic fracture, and wellbore, respectively. Together, these sub-models constitute a complete system, which can more accurately describe the temperature distributions of each component in the shale gas extraction process and their variation rules with time.

Reservoir temperature modeling [45]:

$$\overline{\rho C_p}\frac{\partial T}{\partial t} - \phi\alpha_T T\frac{\partial p}{\partial t} + \frac{k}{\mu}(\alpha_T T - 1)\left[\left(\frac{\partial p}{\partial y}\right)^2 + \left(\frac{\partial p}{\partial z}\right)^2\right] = \frac{\rho k C_p}{\mu}\left(\frac{\partial p}{\partial y}\frac{\partial T}{\partial y} + \frac{\partial p}{\partial z}\frac{\partial T}{\partial z}\right) + \eta\left(\frac{\partial^2 T}{\partial x^2} + \frac{\partial^2 T}{\partial y^2} + \frac{\partial^2 T}{\partial z^2}\right) \tag{17}$$

Hydraulic crack temperature modeling [46]:

$$\overline{\rho C_p}\frac{\partial T_F}{\partial t} - \phi_F \alpha_T T_F + \frac{k_F}{\mu_g}(\alpha_T T_F - 1)\left[\left(\frac{\partial p_F}{\partial x}\right)^2 + \left(\frac{\partial p_F}{\partial z}\right)^2\right] = \frac{\rho k_F C_p}{\mu_g}\left(\frac{\partial p_F}{\partial x}\frac{\partial T_F}{\partial x} + \frac{\partial p_F}{\partial z}\frac{\partial T_F}{\partial z}\right) + \eta_F\left(\frac{\partial^2 T_F}{\partial y^2} + \frac{\partial^2 T_F}{\partial z^2}\right) \quad (18)$$

Wellbore temperature modeling:

$$\frac{1}{v}\frac{\partial T_{wb}}{\partial t} - \frac{\alpha_T T_{wb}}{\rho v C_p}\frac{\partial p_{wb}}{\partial t} = \frac{2\gamma\rho_I v_I}{R_{inw}\rho v}(T_I - T_{wb}) - \frac{\partial T_{wb}}{\partial y} + \frac{2(1-\gamma)}{R_{inw}\rho v C_p}U_T(T_I - T_{wb}) + k_{JT}\frac{\partial p_{wb}}{\partial y} - \frac{g\sin\theta}{C_p} \quad (19)$$

where C_p represents the specific heat capacity of the shale and fluid, ρ represents the density of the shale and fluid, k represents the reservoir permeability, k_F represents the artificial fracture permeability, T represents the reservoir temperature, T_F represents the artificial fracture temperature, and η represents the thermal conductivity of the reservoir. η_F represents the thermal conductivity of the artificial fracture, p represents the reservoir pressure, p_F represents the artificial fracture pressure, T_I represents the fluid temperature flowing into the wellbore from the artificial fracture, and γ represents the opening degree of the wellbore. T_{wb} is the temperature in the wellbore, U_T is the comprehensive heat transfer coefficient, k_{JT} is the Joule–Thomson coefficient, ρ_I represents the density of the fluid flowing into the wellbore from the artificial fracture, and ν_I is the flow rate of the fluid flowing into the wellbore from the artificial fracture.

4. Model Solution

To predict the temperature distribution in shale gas horizontal wells using the finite difference method, it is essential to thoroughly evaluate the coupling effects among the temperature, seepage, and stress fields (as depicted in Figure 2). The finite difference method, a numerical solution technique, involves discretizing spatial and temporal domains and iteratively approximating the true solution.

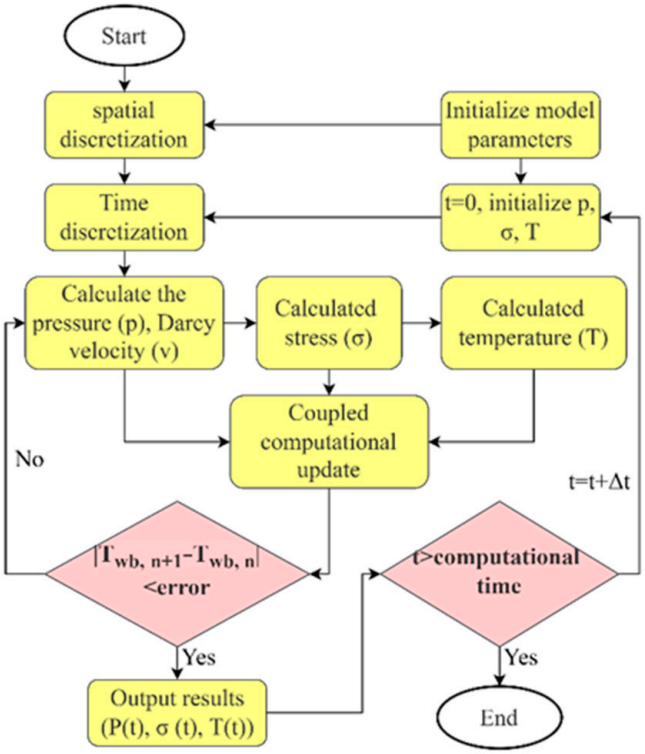


Figure 2. Flow chart for solving the horizontal well temperature prediction model.

The process begins by defining the geometric layout of the wellbore, fractures, and reservoir, followed by inputting the physical properties of the rock and fluid. The initial conditions and boundary constraints for the temperature, pressure, and stress fields are then specified. The model domain is discretized into a network of spatial nodes, and an appropriate time step is selected to ensure computational stability and accuracy.

Next, the governing equations for seepage Equation (16), solid mechanics Equation (4), and heat transfer Equations (17)–(19) are discretized to determine the distributions of the seepage, stress, and temperature fields, respectively. During this process, it is crucial to account for the feedback mechanisms among the three fields, continuously updating their attributes to reflect these interactions. The iterative calculations proceed until the convergence criteria are met, such that changes in pressure, stress, and temperature fall below the predefined thresholds.

Ultimately, the results provide the distributions of the pressure, stress, and temperature fields, enabling an in-depth analysis of their evolution during gas extraction. These findings offer theoretical insights to support the optimization of shale gas production.

5. Model Verification

The present study focuses on the Marcellus Shale reservoir, employing a systematic evaluation approach through a staged validation process. Firstly, the simplified model was validated without considering the stress field effect. This was based on the reservoir's physical parameters listed in Table 1 and the production dynamic data provided by the literature [47,48]. Subsequently, a numerical simulation study was conducted by applying the thermo-hydro-mechanical full-coupling model established in this paper. The effect of the stress coupling effect on the production capacity prediction was quantitatively analyzed by comparing the prediction results of the simplified model and the full-coupling model with the actual production data (see Figure 3).

Table 1. Parameters associated with Marcellus shale gas reservoirs.

Parameter	Value	Unit
Simulation model dimension	$609.6 \times 152.4 \times 52.7$	m
Initial reservoir pressure, p_0	3.45×10^7	Pa
Bottom hole pressure, p_w	2.4×10^6	Pa
Langmuir pressure, P_L	3×10^6	Pa
Langmuir volume, V_L	2.5×10^{-3}	m^3/kg
Reservoir temperature, T	352	K
Initial matrix permeability, k_0	1×10^{-19}	m^2
Initial matrix porosity, Φ_0	0.03	
Young's modulus of shale, E	3×10^{10}	Pa
Poisson's ratio	0.2	
Surface diffusion coefficient	1×10^{-8}	m^2/s
Horizontal well length	426.7	m
Number of fractures	14	
Hydraulic fracture half-length	85	m
Hydraulic fracture spacing	30.5	m

During the initial phase of shale gas extraction, the output rates indicate a rapid decrease following a brief peak. In the later phases, due to the extended nature of gas desorption and the diffusion processes inside the shale matrix, the rate of production efficiency further drops, but the pace of decline slows dramatically. Interestingly, omitting the stress field effect in the calculations leads to an overestimation of production by around 12.9%. In contrast, the full-coupled model displays an enhanced accuracy of 5.6%, correlating more

closely with actual field data. This comparison substantiates the validity and usefulness of the fully coupled model for predicting shale gas production behavior.

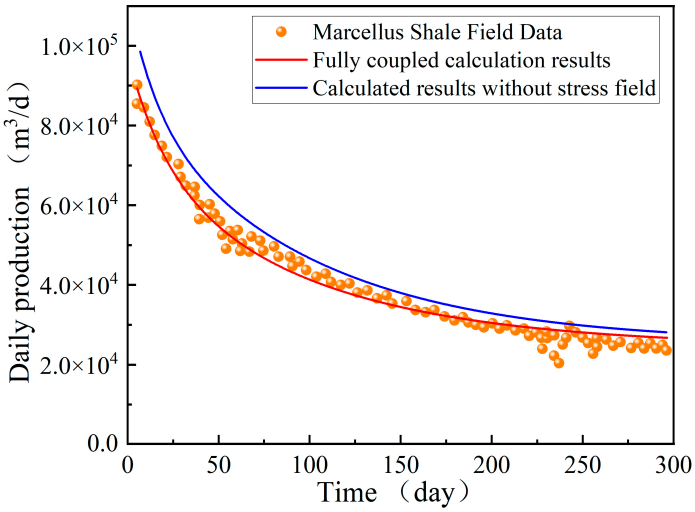


Figure 3. Comparison of numerical results with actual data.

6. Results and Discussion

6.1. Coupled Model Calculation Results

Figure 4 demonstrates the pressure distribution, stress state, and temperature field evolution characteristics of the fractured zone in a 400 m horizontal section of a horizontal well during different time phases. In the process of shale gas horizontal well production, with the steady decrease of pressure in the well, shale gas seeps from matrix pores and fractures to the wellbore due to the drive of the pressure gradient. In the early stage of production, due to the considerable pressure difference between the reservoir and the wellbore, the seepage rate is faster and predominantly concentrated in the area near the fractures. As shale gas production continues, on the one hand, the pressure of the reservoir gradually decreases, resulting in a reduction of the pressure gradient, which slows down the seepage rate; on the other hand, the desorption of gas reduces the gas content in the matrix pore space, and at the same time, the permeability of the matrix changes, which in turn affects the seepage process.

Due to the drop in pore pressure, the effective stress in the rock mass increases, resulting in the deformation of the shale. In the early phases of shale gas production, the most important changes in stress occur in the wellbore and in the areas near the fractures, which may lead to fracture closure or deformation. As the production period increases, the stress experienced by deep geological structures also undergoes a shift. When these stresses exceed the strength limit of the rock, new microfractures may be produced or lead to the expansion of existing fractures, and this modification further influences the seepage and temperature fields [49–51].

At the same time, the pressure differential encourages quick the desorption and diffusion of shale gas and its flow from the reservoir to the wellbore. This process is accompanied by heat absorption, resulting in a rapid fall in temperature in the region of the wellbore. Thermal convection causes the cooled gas (desorbed shale gas) to exchange heat with the surrounding rocks and fluids, resulting in a steady outward spread of the lower temperature zone. With the continuation of the extraction time, the overall temperature of the reservoir continues to fall, but the rate of cooling gradually slows down.

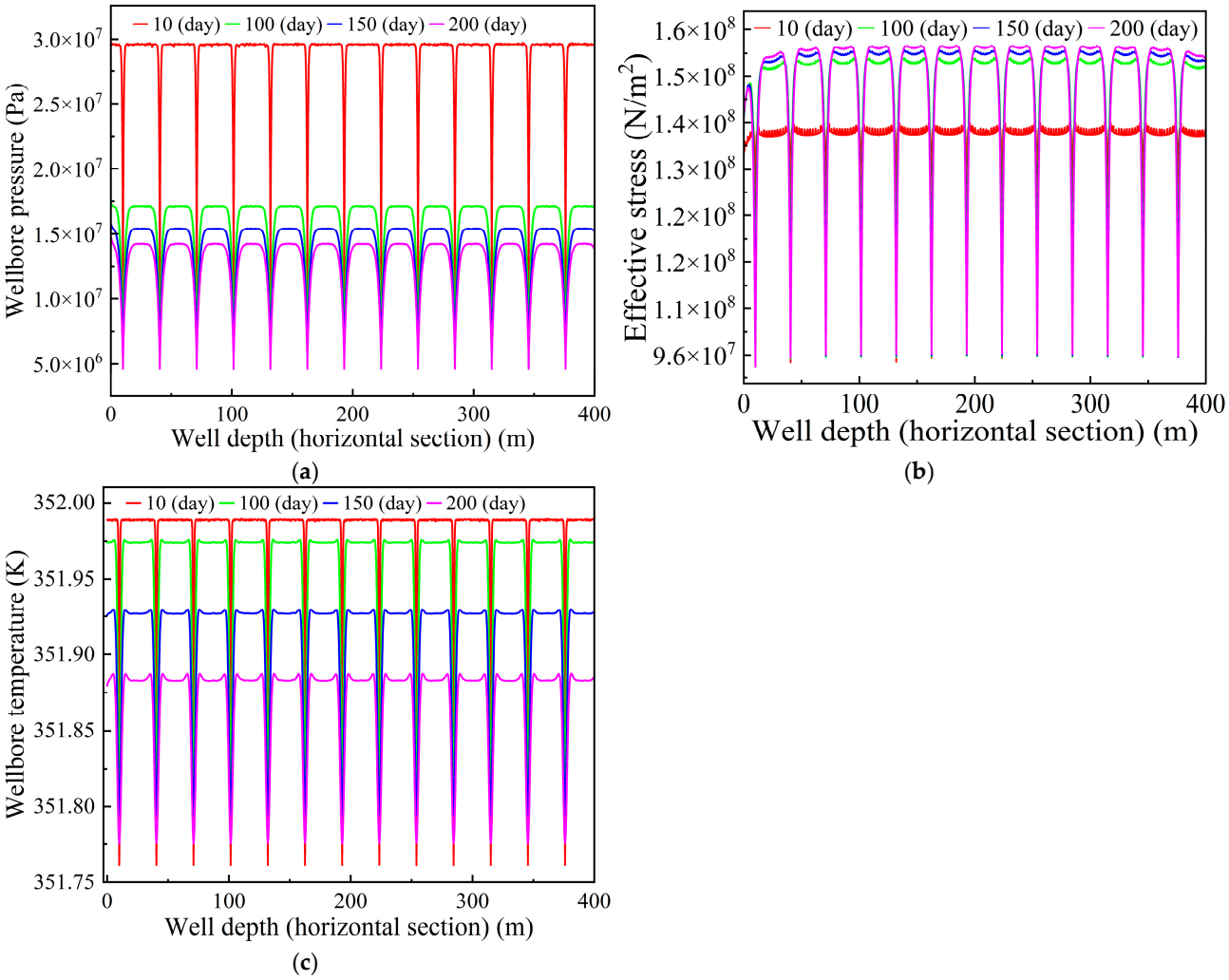


Figure 4. Pressure distribution, stress distribution, and temperature distribution at different points during the production process. (**a**) Pressure change curve. (**b**) Stress change curve. (**c**) Temperature change curve.

6.2. Sensitivity Analysis of Stress Parameters

6.2.1. Effect of Porosity on Wellbore Temperature

In the coupled multi-physical field model, the wellbore temperature distribution was simulated and analyzed by assuming the reservoir porosity to be 0.02, 0.025, 0.03, 0.035, and 0.04, respectively, while leaving the other parameters constant. The results demonstrate that during the extraction process, the fall of gas pressure triggers the gas expansion effect, which leads to a decrease in the local temperature. It is obvious that with an increase in reservoir porosity, there is a large expansion of the gas flow channels and storage capacity within the reservoir. Consequently, the gas release rate and expansion effect become progressively pronounced. This event may result in an enhancement of the amplitude of the temperature drop in the fracture area (as demonstrated in Figure 5a). Furthermore, Figure 5b indicates the amount of temperature fall in the fracture region and the trend of wellbore temperature under varied porosity circumstances.

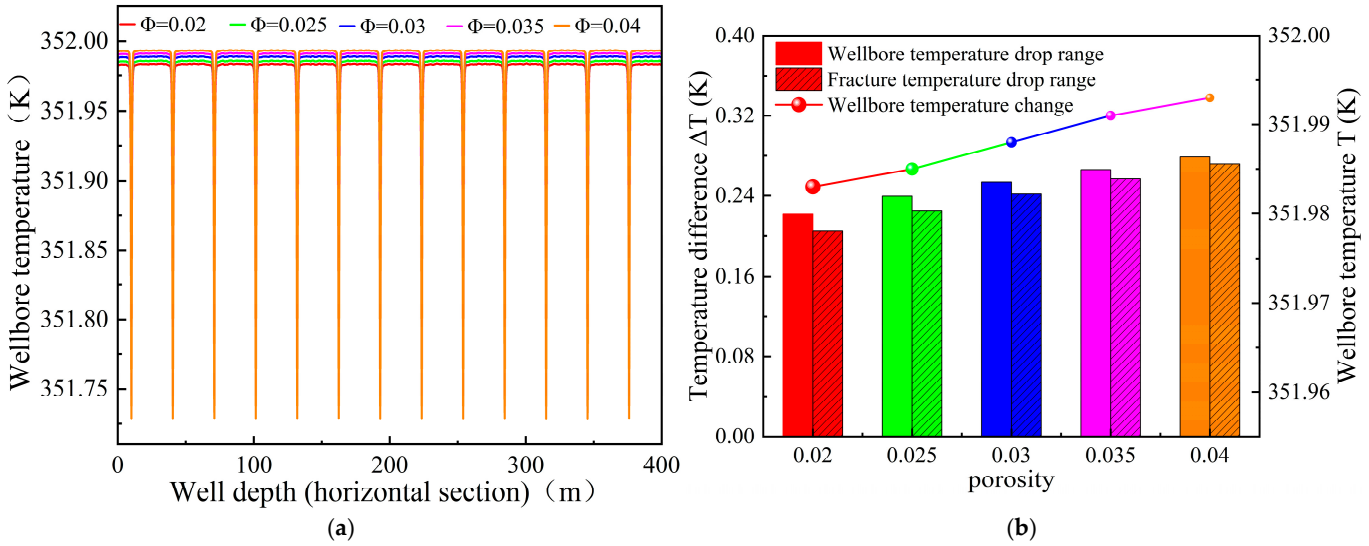


Figure 5. Effect of porosity on wellbore temperature. (**a**) Temperature distribution in the wellbore. (**b**) Magnitude of temperature change.

6.2.2. Influence of Permeability on Wellbore Temperature

As illustrated in Figure 6, the impact of varying permeabilities on wellbore temperature is demonstrated. In circumstances where permeability is minimal, the flow of gas is impeded, the rate of gas release is diminished, and the impact of gas expansion is negligible. The predominant function of heat conduction is evident, leading to a gradual decline in temperature in the vicinity of the wellbore, with a relatively limited range of temperature reduction. Conversely, an increase in permeability leads to the enhancement of the flow channels within the reservoir, thereby accelerating the gas flow rate and amplifying the gas release and expansion effects. This heightened expansion action exerts a significant heat absorption capacity, resulting in a rapid temperature reduction surrounding the wellbore. However, with the passage of time and the progression of shale gas production, the temperature decline impact tends to stabilize.

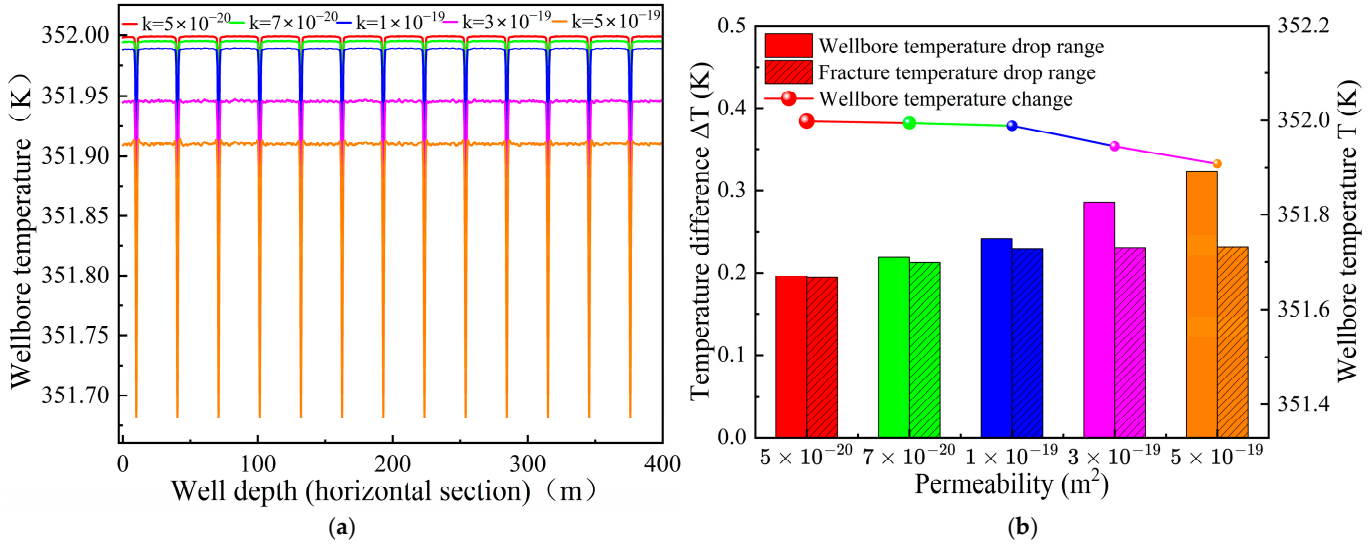


Figure 6. Effect of permeability on wellbore temperature. (**a**) Wellbore temperature distribution. (**b**) Magnitude of temperature change.

6.2.3. Effect of Young's Modulus on Wellbore Temperature

As illustrated in Figure 7, the effect of varying Young's moduli on wellbore temperature is demonstrated. When Young's modulus is minimal, the rock exhibits reduced rigidity and augmented elasticity, leading to enhanced crack deformation and increased crack vulnerability. Consequently, the inflow capacity is elevated. Consequently, the gas flow is more uniform, the wellbore pressure drop is diminished, the gas expansion cooling effect is diminished, and the wellbore temperature is augmented. Conversely, an increase in Young's modulus results in an enhancement of rock rigidity, a reduction in fracture deformation capacity, an acceleration in fracture closure following a fracturing, and a significant decrease in fracture flow-conducting capacity. Consequently, the gas flow rate from the reservoir to the wellbore is reduced, while the wellbore pressure drop is increased. The enhanced pressure drop in the wellbore leads to an augmented cooling effect of gas expansion, consequently resulting in a further decline in the wellbore temperature.

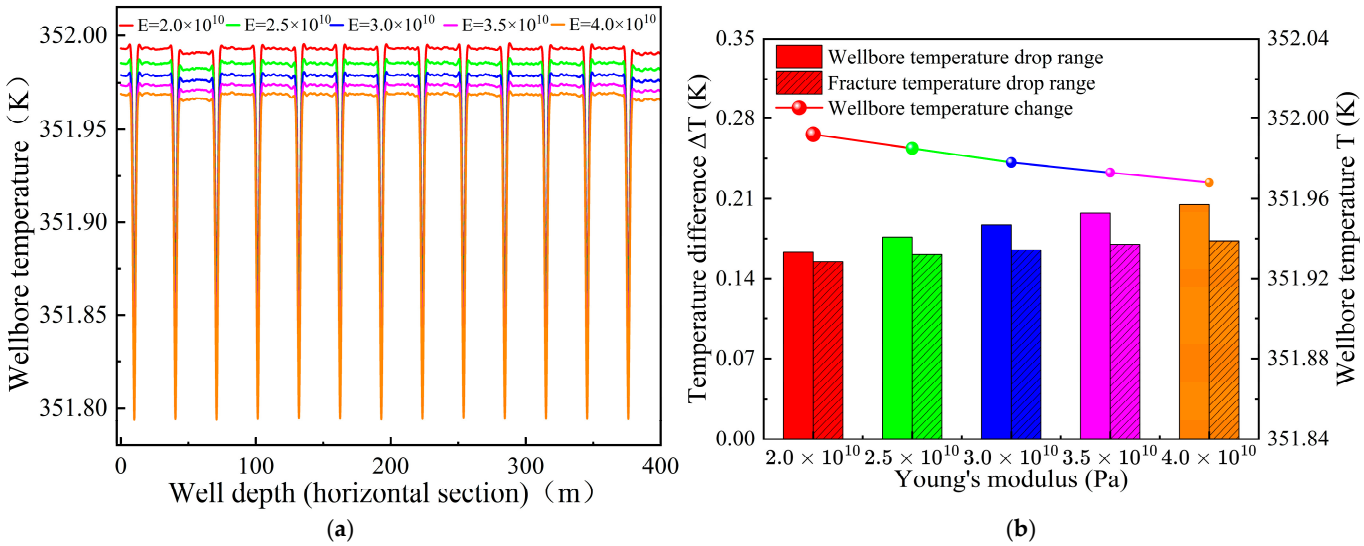


Figure 7. Effect of Young's modulus on wellbore temperature. (**a**) Wellbore temperature distribution. (**b**) Magnitude of temperature change.

6.2.4. Effect of Langmuir Pressure on Wellbore Temperature

As indicated in Figure 8, the effect of changing the Langmuir pressures on wellbore temperature is illustrated. As the reservoir pressure approaches the Langmuir pressure, the lower Langmuir pressure implies that the gas can start desorbing at a lower reservoir pressure and is accompanied by a greater amount of desorption. Due to the strong cooling effect during gas expansion, the heat absorption is enhanced, which results in a quick drop in temperature near the wellbore. Conversely, an increase in the Langmuir pressure necessitates a higher reservoir pressure for efficient gas desorption, hence delaying the desorption rate and lowering the gas release under constant wellbore pressure conditions. This, in turn, leads to a diminished expansion cooling effect and a reduced temperature drop near the wellbore.

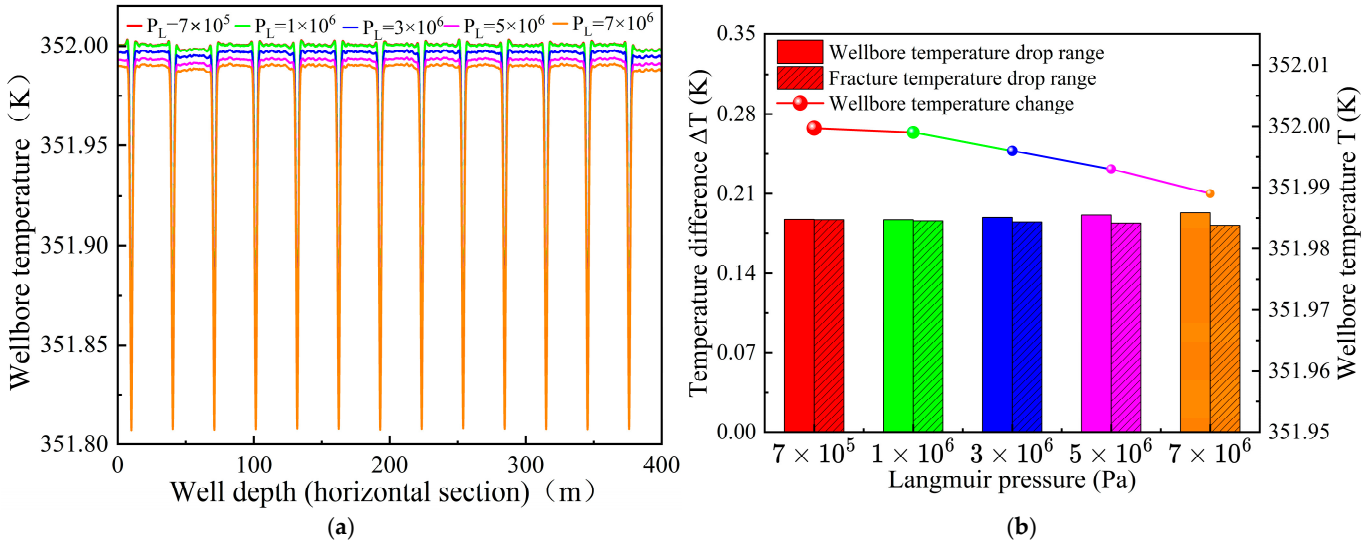


Figure 8. Effect of Langmuir pressure on wellbore temperature. (**a**) Wellbore temperature distribution. (**b**) Magnitude of temperature change.

6.2.5. Effect of Langmuir Volume on Wellbore Temperature

Figure 9 demonstrates the law of the effect of different Langmuir volumes on the wellbore temperature. When the Langmuir volume is small, the amount of adsorbed gas in the reservoir is limited, and the desorption of the gas under the bucking condition is small, resulting in the gas expansion effect and the corresponding heat absorption effect in the reservoir being not significant. Therefore, the temperature drop in the wellbore and its neighboring area is small. With the increase of the Langmuir volume, the storage capacity of the reservoir for adsorbed gas is enhanced, and more desorbed gas can be released into the fracture and wellbore during the buckling process, and the rate of desorption is then accelerated. The large amount of the desorption and expansion effect of the gas significantly enhanced the heat absorption process, resulting in a significantly larger temperature drop in the wellbore and the area around the fracture.

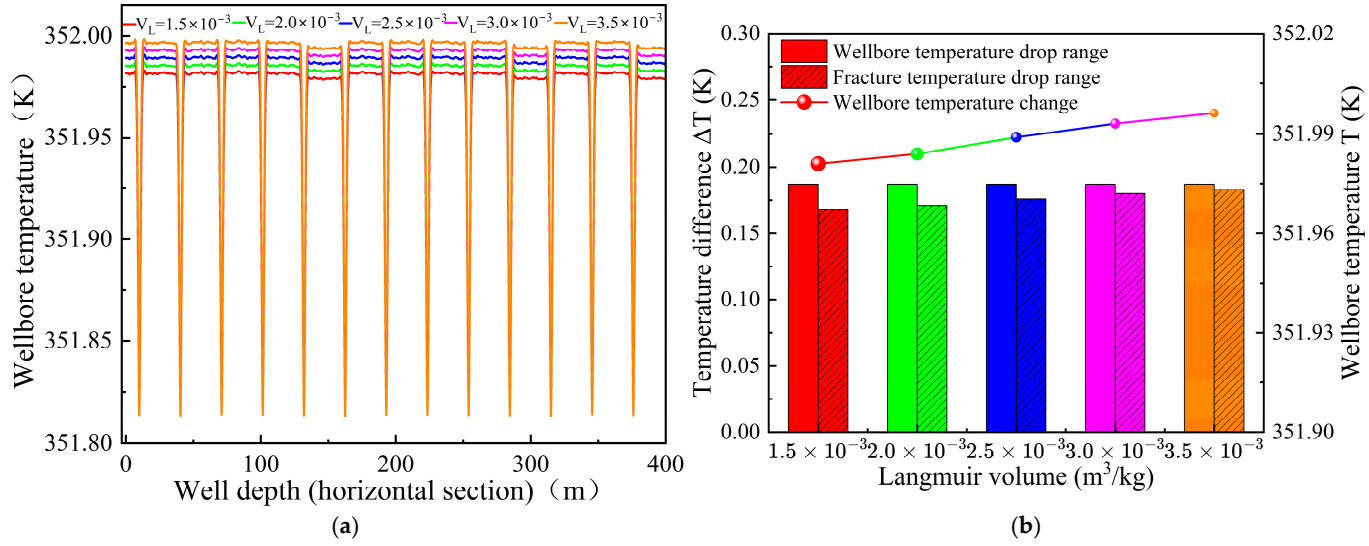


Figure 9. Effect of Langmuir volume on wellbore temperature. (**a**) Wellbore temperature distribution. (**b**) Magnitude of temperature change.

6.2.6. Effect of Adsorption Strain on Wellbore Temperature

As indicated in Figure 10, the effect of different adsorption strains on wellbore temperature is illustrated. Changes in adsorption strain have been found to generate modifications in pore structure due to the expansion or contraction of the reservoir matrix during gas desorption. An increase in adsorption strain has been shown to result in matrix deformation, which has been demonstrated to enhance the compression effect of the pores, reducing reservoir permeability and impeding gas flow. This, in turn, can lead to a further reduction of the efficiency of the heat–mass exchange between the gas and the wellbore surroundings, which may result in a decrease in the wellbore temperature. Additionally, it is vital to note that shale gas desorption is a process of heat absorption, and an increase in adsorption strain will boost the desorption impact. This, in turn, might worsen the fall in local reservoir temperature and, thus, indirectly affect the wellbore temperature. Consequently, the enhancement of desorption's thermal effect, concurrent with an increase in adsorption strain, may culminate in a further fall in the wellbore temperature.

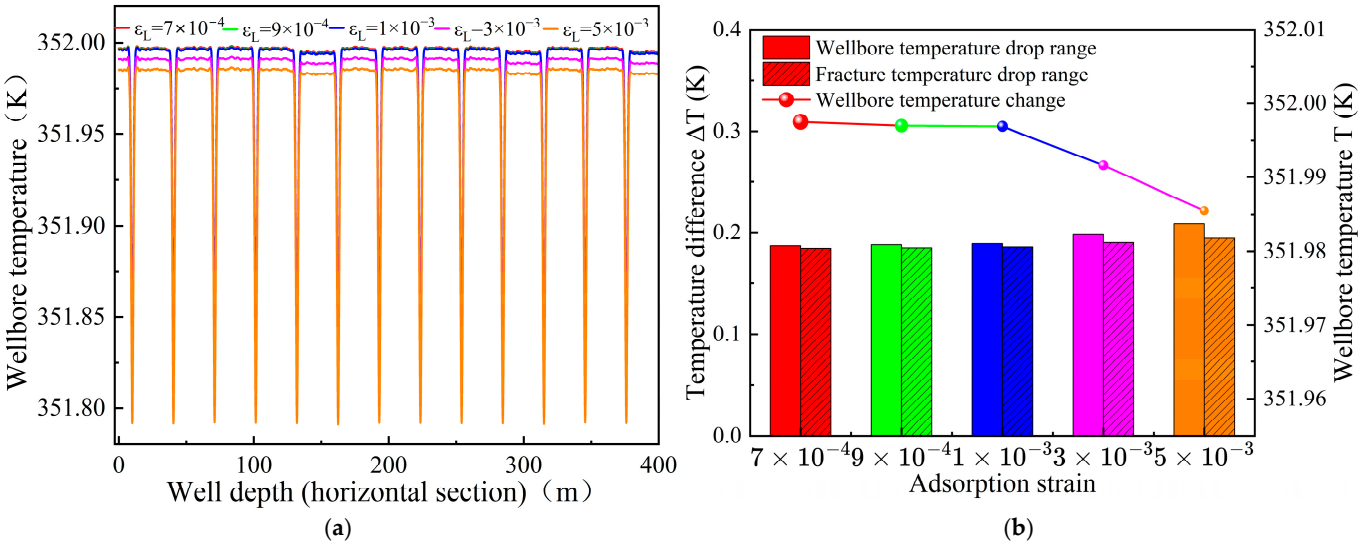


Figure 10. Effect of adsorption strain on wellbore temperature. (**a**) Wellbore temperature distribution. (**b**) Magnitude of temperature change.

6.2.7. Effect of Coefficient of Thermal Expansion on Wellbore Temperature

Figure 11 demonstrates the influence of different coefficients of thermal expansion on the wellbore temperature. As the coefficient of thermal expansion increases, the volume change of the gas becomes more sensitive to the temperature, which intensifies the Joule–Thomson effect (JT effect) that occurs during the flow and depressurization of the gas. Larger thermal expansion coefficients impair the temperature gradient shift of the gas, further enhancing the heat–mass exchange between the wellbore and the surrounding rock formation. In addition, the gas expansion effect paired with heat absorption and desorption makes the reservoir's sensitivity to temperature changes more critical, which may lead to local pore structure changes and reduce heat and mass transmission efficiency. Overall, as the coefficient of thermal expansion increases, the wellbore temperature decline increases, and the rate of temperature reduction may accelerate.

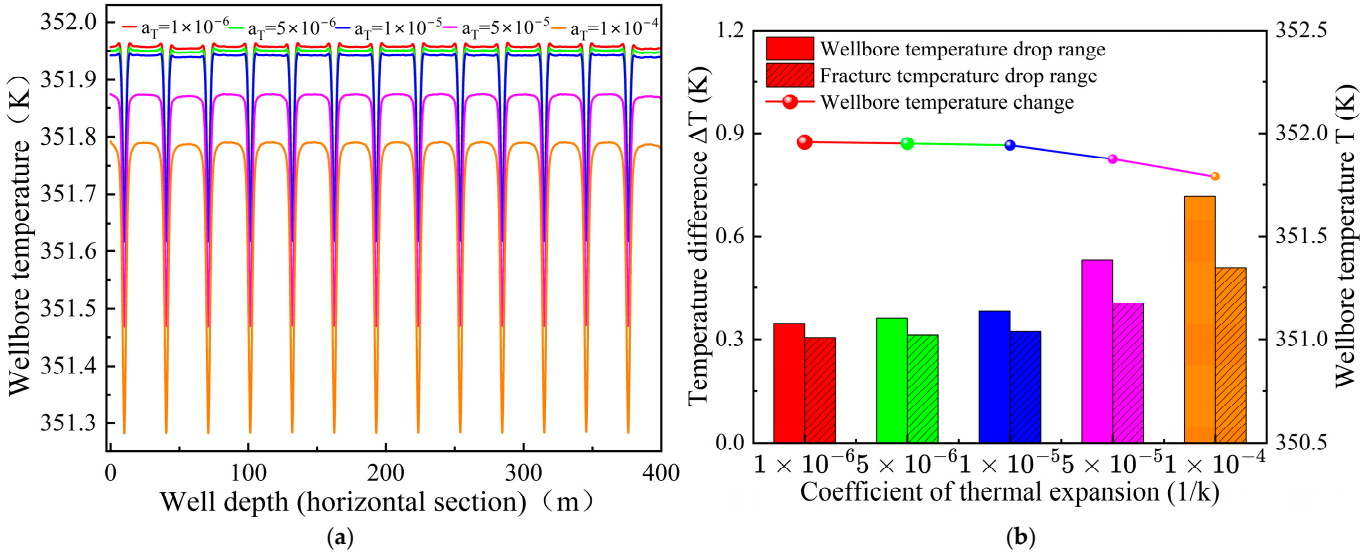


Figure 11. Effect of coefficient of thermal expansion on wellbore temperature. (**a**) Wellbore temperature distribution. (**b**) Magnitude of temperature change.

7. Conclusions

In this study, we focus on the effect of reservoir stress field sensitivity on the coupled thermo-hydro-mechanical process and construct a horizontal well temperature prediction model that comprehensively considers the interactions of thermodynamics, fluid dynamics, and solid mechanics in the shale gas extraction process. The accuracy of the model is verified by comparing and analyzing the model calculation results with the measured data in the field, and a sensitivity analysis of seven stress-related uncertain parameters is executed. The model calculations yielded the following main conclusions:

(1) It has been demonstrated that stress field-related parameters have the capacity to exert influence upon the dynamic distribution of wellbore temperature during gas desorption, diffusion, and seepage extraction driven by pressure differences.

(2) The coupled thermo-hydro-mechanical model can more accurately predict the dynamics of wellbore temperatures, thus significantly improving the accuracy of shale gas production predictions. Neglecting the stress field effect may lead to an overestimation of shale gas production by up to 12.9%.

(3) The porosity and Langmuir volume of the reservoir are positively correlated with the wellbore temperature, whereas permeability, Young's modulus, Langmuir pressure, the coefficient of thermal expansion, and adsorption strain are negatively correlated with the wellbore temperature.

Author Contributions: Conceptualization, J.L. and D.Y.; methodology, Q.D. and F.W.; software, J.L.; validation, H.H. and D.P.; formal analysis, D.Y. and F.W.; investigation, J.L.; writing—original draft preparation, J.L.; writing—review and editing, H.H., Q.D. and D.P. All authors have read and agreed to the published version of the manuscript.

Funding: This study was funded by the Hubei Outstanding University Science and Technology Innovation Program Team, No. 7111104202.

Data Availability Statement: The original contributions presented in this study are included in the article. Further inquiries can be directed to the corresponding author.

Acknowledgments: We would like to express our sincere gratitude to the editors and reviewers for their constructive feedback and the time and effort they dedicated to the review process.

Conflicts of Interest: The authors declare no conflicts of interest.

References

1. Liu, W.; Ramirez, A. State of the Art Review of the Environmental Assessment and Risks of Underground Geo-Energy Resources Exploitation. *Renew. Sustain. Energy Rev.* **2017**, *76*, 628–644. [CrossRef]
2. Zhao, M.; Yuan, B.; Liu, Y.; Zhang, W.; Zhang, X.; Guo, W. Dynamic Prediction of Fracture Propagation in Horizontal Well Hydraulic Fracturing: A Data-Driven Approach for Geo-Energy Exploitation. *Geoenergy Sci. Eng.* **2024**, *241*, 213182. [CrossRef]
3. Song, Y.; Zhang, D.; Ranjith, P.G.; Huang, Y.; Wu, B.; Zhang, F.; Kong, L.; Perera, M.S.A. Critical Review of DEM Simulation for Sand Production during Geo-Energy Development: Models, Parameters, and Future Directions. *Powder Technol.* **2024**, *444*, 119977. [CrossRef]
4. Wu, Z.; Cui, C.; Yang, Y.; Zhang, C.; Wang, J.; Cai, X. A Fractal Permeability Model of Tight Oil Reservoirs Considering the Effects of Multiple Factors. *Fractal Fract.* **2022**, *6*, 153. [CrossRef]
5. Zhu, C.; Yang, S.; Pu, Y.; Sun, L.; Wang, M.; Du, K. Advanced Progress of the Geo-Energy Technology in China. *Energies* **2023**, *16*, 6812. [CrossRef]
6. Mokhtari, R.; Anabaraonye, B.U.; Afrough, A.; Mohammadkhani, S.; Feilberg, K.L. Experimental Investigation of Low Salinity Water-Flooding in Tight Chalk Oil Reservoirs. *J. Pet. Sci. Eng.* **2022**, *208*, 109282. [CrossRef]
7. Wang, H.; Xu, L.; Yan, Z.; Gulliver, T.A. Low-Complexity MIMO-FBMC Sparse Channel Parameter Estimation for Industrial Big Data Communications. *IEEE Trans. Ind. Inform.* **2021**, *17*, 3422–3430. [CrossRef]
8. Wang, Q.; Wang, Q.; Zhao, C.; Zhao, J.; Yan, Z.; Kang, S.; Hu, Y.; Ren, L. Numerical Simulation of Planar Hydraulic Fracture Propagation with Consideration to Transition from Turbulence to Laminar Flow Regime. *Eng. Fract. Mech.* **2022**, *262*, 108258.
9. Takeda, M.; Manaka, M.; Tuji, T. Chemical Osmosis as a Cause for the Improved Oil Recovery by Low-Salinity Water Flooding: Experimental and Numerical Approaches for Detection. *J. Pet. Sci. Eng.* **2021**, *207*, 109090. [CrossRef]
10. Wang, H.; Xiao, P.; Li, X. Channel Parameter Estimation of mmWave MIMO System in Urban Traffic Scene: A Training Channel-Based Method. *IEEE Trans. Intell. Transp. Syst.* **2024**, *25*, 754–762. [CrossRef]
11. Wang, Q.; Zhao, J.; Wang, B.; Li, D.; Ran, L.; Hu, Y.; Zhao, C. Secondary Growth and Closure Behavior of Planar Hydraulic Fractures during Shut-In. *J. Pet. Sci. Eng.* **2022**, *213*, 110420. [CrossRef]
12. Kragas, T.K.; Williams, B.A.; Myers, G.A. The Optic Oil Field: Deployment and Application of Permanent In-Well Fiber Optic Sensing Systems for Production and Reservoir Monitoring. In Proceedings of the SPE Annual Technical Conference and Exhibition, New Orleans, LA, USA, 30 September–3 October 2001; OnePetro: Richardson, TX, USA, 2001.
13. Xie, Q.; Wang, Z.; Wen, F.; He, J.; Truong, T.-K. Coarray tensor train decomposition for bistatic MIMO radar with uniform planar array. *IEEE Trans. Antennas Propag.* **2025**, *32*, 46–50. [CrossRef]
14. Cai, J.; Duan, Y. Study on Temperature Distribution along Wellbore of Fracturing Horizontal Wells in Oil Reservoir. *Petroleum* **2015**, *1*, 358–365. [CrossRef]
15. Holley, E.H.; Molenaar, M.M.; Fidan, E.; Banack, B. Interpreting Uncemented Multistage Hydraulic-Fracturing Completion Effectiveness Using Fiber-Optic DTS Injection Data. *SPE Drill Complet.* **2012**, *28*, 243–253. [CrossRef]
16. Tabatabaei, M.; Zhu, D. Fracture-Stimulation Diagnostics in Horizontal Wells Through Use of Distributed-Temperature-Sensing Technology. *SPE Prod. Oper.* **2012**, *27*, 356–362. [CrossRef]
17. Kaeshkov, I.S.; Kremenetskiy, M.I.; Buyanov, A.V. Horizontal Well Monitoring Based on Temperature Profile Measuring with Distributed Temperature Sensors (DST). In Proceedings of the SPE Russian Oil and Gas Exploration & Production Technical Conference and Exhibition, Moscow, Russia, 14–16 October 2014; OnePetro: Richardson, TX, USA, 2014.
18. Malanya, G.; Butula, K.; Burdin, K.; Khaziev, M.; Kuzmin, S.; Kaeshkov, I.; Kremenetskiy, M. Successful Experience of Estimating Injection Flow Profile in Horizontal Wells Completed with Multistage Fracs in Conventional Reservoirs Using CT Conveyed Distributed Temperature Sensing. In Proceedings of the SPE Russian Petroleum Technology Conference and Exhibition, Moscow, Russia, 24–26 October 2016; OnePetro: Richardson, TX, USA, 2016.
19. Wei, C.; Tabjula, J.L.; Sharma, J.; Chen, Y. The Modeling of Two-Way Coupled Transient Multiphase Flow and Heat Transfer during Gas Influx Management Using Fiber Optic Distributed Temperature Sensing Measurements. *Int. J. Heat Mass Transf.* **2023**, *214*, 124447. [CrossRef]
20. Yan, C.; Ren, J.; Shi, Q.; Li, X.; Bai, Y.; Yu, W. Flow Profiling Analysis of a Refractured Tight Oil Well Using Distributed Temperature Sensing. *Processes* **2024**, *12*, 2106. [CrossRef]
21. Luo, H.; Li, H.; Lu, Y.; Li, Y.; Guo, Z. Inversion of Distributed Temperature Measurements to Interpret the Flow Profile for a Multistage Fractured Horizontal Well in Low-Permeability Gas Reservoir. *Appl. Math. Model.* **2020**, *77*, 360–377. [CrossRef]
22. Ramey, H.J., Jr. Wellbore Heat Transmission. *J. Pet. Technol.* **1962**, *14*, 427–435. [CrossRef]
23. Luo, H.; Li, H.; Li, Y.; Lu, Y.; Tan, Y. Investigation of Temperature Behavior for Multi-Fractured Horizontal Well in Low-Permeability Gas Reservoir. *Int. J. Heat Mass Transf.* **2018**, *127*, 375–395. [CrossRef]

24. Cui, J.; Yang, C.; Zhu, D.; Datta-Gupta, A. Fracture Diagnosis in Multiple-Stage-Stimulated Horizontal Well by Temperature Measurements with Fast Marching Method. *SPE J.* **2016**, *21*, 2289–2300. [CrossRef]
25. Yang, S.; Lai, F.; Li, Z.; Fu, Y.; Wang, K.; Zhang, L.; Liang, Y. The Effect of Temperature on Flowback Data Analysis in Shale Gas Reservoirs: A Simulation-Based Study. *Energies* **2019**, *12*, 3751. [CrossRef]
26. Sui, W.; Zhang, D.; Cheng, S.; Zou, Q.; Fu, X.; Ma, Z. Improved DTS Profiling Model for Horizontal Gas Wells Completed with the Open-Hole Multi-Stage Fracturing System. *J. Nat. Gas Sci. Eng.* **2020**, *84*, 103642. [CrossRef]
27. Cao, Z.; Li, P.; Li, Q.; Lu, D. Integrated Workflow of Temperature Transient Analysis and Pressure Transient Analysis for Multistage Fractured Horizontal Wells in Tight Oil Reservoirs. *Int. J. Heat Mass Transf.* **2020**, *158*, 119695. [CrossRef]
28. Zheng, Y.; Liu, J.; Liu, Y.; Shi, D.; Zhang, B. Experimental Investigation on the Stress-Dependent Permeability of Intact and Fractured Shale. *Geofluids* **2020**, *2020*, 8897911. [CrossRef]
29. Wu, Z.; Zuo, Y.; Wang, S.; Sunwen, J.; Liu, L. Experimental Study on the Stress Sensitivity and Influence Factors of Shale under Varying Stress. *Shock Vib.* **2018**, *2018*, 3616942. [CrossRef]
30. Li, Y.; Hu, Z.; Liu, X.; Duan, X. Reasonable Application and Interpretation of Effective Stress Principle in Shale Reservoir Mining. *IOP Conf. Ser. Earth Environ. Sci.* **2020**, *555*, 012070. [CrossRef]
31. Detournay, E.; Cheng, A.H.-D. Fundamentals of Poroelasticity. In *Analysis and Design Methods*; Fairhurst, C., Ed.; Pergamon: Oxford, UK, 1993; pp. 113–171. ISBN 978-0-08-040615-2.
32. Zhao, Y.; Lu, G.; Zhang, L.; Wei, Y.; Guo, J.; Chang, C. Numerical Simulation of Shale Gas Reservoirs Considering Discrete Fracture Network Using a Coupled Multiple Transport Mechanisms and Geomechanics Model. *J. Pet. Sci. Eng.* **2020**, *195*, 107588. [CrossRef]
33. Gao, Q.; Han, S.; Cheng, Y.; Shi, X.; Yan, C. Microscale Thermo-Hydro-Mechanical Modeling of Thermal Recovery of Shale Gas. *Geomech. Energy Environ.* **2023**, *34*, 100462. [CrossRef]
34. Liu, J.; Liang, X.; Xue, Y.; Yao, K.; Fu, Y. Numerical Evaluation on Multiphase Flow and Heat Transfer during Thermal Stimulation Enhanced Shale Gas Recovery. *Appl. Therm. Eng.* **2020**, *178*, 115554. [CrossRef]
35. Li, D.; Wang, Y.; Zeng, B.; Lyu, Q.; Zhou, X.; Zhang, N. Optimization of the Shale Gas Reservoir Fracture Parameters Based on the Fully Coupled Gas Flow and Effective Stress Model. *Energy Sci. Eng.* **2021**, *9*, 676–693. [CrossRef]
36. Dai, C.; Liu, H.; Wang, Y.; Li, X.; Wang, W. A Simulation Approach for Shale Gas Development in China with Embedded Discrete Fracture Modeling. *Mar. Pet. Geol.* **2019**, *100*, 519–529. [CrossRef]
37. Xu, C.; Li, P.; Lu, Z.; Liu, J.; Lu, D. Discrete Fracture Modeling of Shale Gas Flow Considering Rock Deformation. *J. Nat. Gas Sci. Eng.* **2018**, *52*, 507–514. [CrossRef]
38. Yuan, J.; Jiang, R.; Cui, Y.; Xu, J.; Wang, Q.; Zhang, W. The Numerical Simulation of Thermal Recovery Considering Rock Deformation in Shale Gas Reservoir. *Int. J. Heat Mass Transf.* **2019**, *138*, 719–728. [CrossRef]
39. Zhu, G.; Yao, J.; Sun, H.; Zhang, M.; Xie, M.; Sun, Z.; Lu, T. The Numerical Simulation of Thermal Recovery Based on Hydraulic Fracture Heating Technology in Shale Gas Reservoir. *J. Nat. Gas Sci. Eng.* **2016**, *28*, 305–316. [CrossRef]
40. Javadpour, F.; Fisher, D.; Unsworth, M. Nanoscale Gas Flow in Shale Gas Sediments. *J. Can. Pet. Technol.* **2007**, *46*, 10. [CrossRef]
41. Yucel Akkutlu, I.; Fathi, E. Multiscale Gas Transport in Shales With Local Kerogen Heterogeneities. *SPE J.* **2012**, *17*, 1002–1011. [CrossRef]
42. Jiang, J.; Younis, R.M. A Multimechanistic Multicontinuum Model for Simulating Shale Gas Reservoir with Complex Fractured System. *Fuel* **2015**, *161*, 333–344. [CrossRef]
43. Mahmoud, M. Development of a New Correlation of Gas Compressibility Factor (Z-Factor) for High Pressure Gas Reservoirs. *J. Energy Resour. Technol.* **2013**, *136*, 012903. [CrossRef]
44. Lee, A.L.; Gonzalez, M.H.; Eakin, B.E. The Viscosity of Natural Gases. *J. Pet. Technol.* **1966**, *18*, 997–1000. [CrossRef]
45. Luo, H.; Li, H.; Zhou, X.; Li, Y.; Li, Y.; Zhu, X. Modeling Temperature Behavior of Multistage Fractured Horizontal Well with Two-Phase Flow in Low-Permeability Gas Reservoirs. *J. Pet. Sci. Eng.* **2019**, *173*, 1187–1209. [CrossRef]
46. Li, H.; Luo, H.; Xiang, Y.; Li, Y.; Jiang, B.; Cui, X.; Gao, S.; Zou, S.; Xin, Y. DTS Based Hydraulic Fracture Identification and Production Profile Interpretation Method for Horizontal Shale Gas Wells. *Nat. Gas Ind. B* **2021**, *8*, 494–504. [CrossRef]
47. Cao, P.; Liu, J.; Leong, Y.-K. A Fully Coupled Multiscale Shale Deformation-Gas Transport Model for the Evaluation of Shale Gas Extraction. *Fuel* **2016**, *178*, 103–117. [CrossRef]
48. Geng, L.; Li, G.; Wang, M.; Li, Y.; Tian, S.; Pang, W.; Lyu, Z. A Fractal Production Prediction Model for Shale Gas Reservoirs. *J. Nat. Gas Sci. Eng.* **2018**, *55*, 354–367. [CrossRef]
49. Gong, X.; Ma, X.; Liu, Y. Analysis of Geological Factors Affecting Propagation Behavior of Fracture during Hydraulic Fracturing Shale Formation. *Geomech. Geophys. Geo-Energy Geo-Resour.* **2024**, *10*, 102. [CrossRef]

50. Min, K.-B.; Rutqvist, J.; Tsang, C.-F.; Jing, L. Stress-Dependent Permeability of Fractured Rock Masses: A Numerical Study. *Int. J. Rock Mech. Min. Sci.* **2004**, *41*, 1191–1210. [CrossRef]
51. Chang, Z.; Zhang, W.; Zhao, G.; Dong, F.; Geng, X. Aging Stability Analysis of Slope Considering Cumulative Effect of Freeze–Thaw Damage—A Case Study. *Minerals* **2022**, *12*, 598. [CrossRef]

Disclaimer/Publisher's Note: The statements, opinions and data contained in all publications are solely those of the individual author(s) and contributor(s) and not of MDPI and/or the editor(s). MDPI and/or the editor(s) disclaim responsibility for any injury to people or property resulting from any ideas, methods, instructions or products referred to in the content.